Accepted Manuscript

Design, synthesis, biological evaluation, and molecular modeling studies of chalcone-rivastigmine hybrids as cholinesterase inhibitors

Ling Wang, Yu Wang, Yiguang Tian, Jinling Shang, Xiaoou Sun, Hongzhuan Chen, Hao Wang, Wen Tan

PII: S0968-0896(16)31102-6
DOI: http://dx.doi.org/10.1016/j.bmc.2016.11.002
Reference: BMC 13368

To appear in: *Bioorganic & Medicinal Chemistry*

Received Date: 7 August 2016
Revised Date: 31 October 2016
Accepted Date: 1 November 2016

Please cite this article as: Wang, L., Wang, Y., Tian, Y., Shang, J., Sun, X., Chen, H., Wang, H., Tan, W., Design, synthesis, biological evaluation, and molecular modeling studies of chalcone-rivastigmine hybrids as cholinesterase inhibitors, *Bioorganic & Medicinal Chemistry* (2016), doi: http://dx.doi.org/10.1016/j.bmc.2016.11.002

Design, synthesis, biological evaluation, and molecular modeling studies of chalcone-rivastigmine hybrids as cholinesterase inhibitors

Ling Wang [a,‡,*], Yu Wang [b,‡], Yiguang Tian [a, ‡,1], Jinling Shang [a], Xiaoou Sun [a], Hongzhuan Chen [b], Hao Wang [b,*], Wen Tan [a,*]

[a]*Guangdong Provincial Key Laboratory of Fermentation and Enzyme Engineering, Pre-Incubator for Innovative Drugs & Medicine, School of Bioscience and Bioengineering, South China University of Technology, Guangzhou 510006, China*

[b]*Department of Pharmacology, Institute of Medical Sciences, Shanghai Jiao Tong University, School of Medicine, 280 South Chongqing Road, Shanghai 200025, China*

[‡]Equal contribution

*Corresponding author:

lingwang@scut.edu.cn (L. Wang)

went@scut.edu.cn (W. Tan);

angela_wanghao@hotmail.com (H. Wang);

Abstract

A series of novel chalcone-rivastigmine hybrids were designed, synthesized, and tested in vitro for their ability to inhibit human acetylcholinesterase and butyrylcholinesterase. Most of the target compounds showed hBChE selective activity in the micro- and submicromolar ranges. The most potent compound **3** exhibited comparable IC_{50} to the commercially available drug (rivastigmine). To better understand their structure activity relationships (SAR) and mechanisms of enzyme-inhibitor interactions, kinetic and molecular modeling studies including molecular docking and molecular dynamics (MD) simulations were carried out. Furthermore, compound **3** blocks the formation of reactive oxygen species (ROS) in SH-SY5Y cells and shows the required druggability and low cytotoxicity, suggesting this hybrid is a promising multifunctional drug candidate for Alzheimer's disease (AD) treatment.

Keywords

Cholinesterase inhibition, chalcone-rivastigmine hybrids, Alzheimer's disease, antioxidative, molecular docking

1. Introduction

Alzheimer's disease (AD) is a debilitating and fatal progressive neurodegenerative disorder always resulting in death over a course that varies from 3 to 20 years.[1] Although the etiology of AD is not yet entirely known, some factors are reported to play key roles in the pathogenesis of this disease, including protein misfolding and aggregation, oxidative stress, mitochondrial abnormalities, neuroinflammation, neuronal toxicity, and low levels of neurotransmitter acetylcholine (ACh).[2-4]

According to the cholinergic hypothesis for AD pathogenesis, the cognitive impairments in AD correlated with cholinergic deficits such as reduced choline acetyltransferase (ChAT) activity and synaptic acetylcholine synthesis.[5] These observations were made just as the role of the cholinergic system in memory processing and learning began to be more widely appreciated.[6] At the neuronal level, ACh can be degraded by two types of cholinesterase enzymes: acetylcholinesterase (EC 3.1.1.7; AChE) and butyrylcholinesterase (EC 3.1.1.8; BChE). AChE is mainly expressed by neurons and its activity is dominant in the healthy brain (80%), while BChE activity is mainly associated with glial cells and seems to play only a supportive role in the healthy brain.[7] Due to the extraordinary efficiency and the classical relationship between AChE and the neurotransmitter acetylcholine, AChE has been a drug target for the treatment of AD. Over the past 20 years, several AChE inhibitors have been launched on the market for AD treatment, including tacrine, donepezil, rivastigmine, and the alkaloid galanthamine (Figure 1). These drugs had made an important contribution to the management and well-being of early stage AD patients. However, significant scientific and clinical questions about AChE inhibitors remain unsolved, e.g., lacking the efficacy for late stage AD patients,[8] peripheral side effects,[9] and the rapid emergence of drug resistance.[10, 11]

In contrast to AChE, BChE is found ubiquitously throughout the human body and BChE knockout mice show no physiological Alterations.[12] The characterization of

AChE nullizygote (AChE -/-) mouse with a clear phenotype appears to have normal CNS function, demonstrating that BChE can rescue the cholinergic function in the absence of AChE.[13] This finding is consistent with previous studies that exhibited an increase of BChE expression in the brain to compensate the loss of AChE activity during AD progression. Furthermore, silent BChE mutations in humans show a slower rate of cognitive decline.[14] Selective BChE inhibitors, cymserine analogs, could elevate extracellular ACh levels and augment long-term potentiation and learning in AD model rats.[15] A notable feature of cymserine analogs was the absence of peripheral side effects associated with AChE inhibitors.[15] Increasing evidence for the involvement of BChE in AD supports it as a promising drug target for AD treatment.

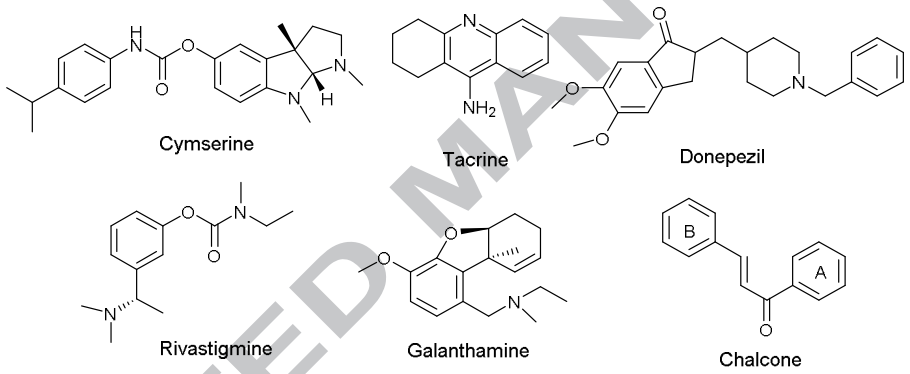

Figure 1. Chemical structures of ChE ligands and chalcone.

Rivastigmine (Figure 1), a newer-generation inhibitor approved in 2000 under the name of Exelon, with a dual inhibitory action on both AChE and BChE, has demonstrated broad benefits across the severity of AD and also in patients with Lewy body variant of AD.[16, 17] Compared with other commercial AChE inhibitors, rivastigmine is a relative weak AChE and BChE inhibitor because of its specific inhibitory mechanism of the carbamate structure encoded in rivastigmine as slow substrate reacting covalently with the active site of the AChE and BChE.[18] Previous experimental and computational studies demonstrate that the carbamate structure of rivastigmine is a necessary pharmacophore for *in vitro* and *in vivo* peculiar pharmacological profiles which are benefited from the ability to inhibit BChE in

addition to AChE.[19, 20] Chalcones (trans-1,3-diphenyl-2-propen-1-ones, Figure 1), the biogenetic precursors of flavonoids and isoflavonoids, are abundant in edible plants[21]. They display a broad spectrum of pharmacological activities such as antioxidative, anticancer, anti-inflammatory, antimalarial, antifungal, antilipidemic, and antiviral activities.[21-24] Some chalcone derivatives also exhibit potent activity against amyloid-β aggregation and 5-lipoxygenase, suggesting that chalcone derivatives can be considered as multifunctional agents for AD treatment.[25]

In the present study, combining both the rivastigmine and chalcones, we designed, synthesized, and evaluated chalcone-rivastigmine hybrids as inhibitors of AChE and BChE. Their structure activity relationships (SAR) and mechanisms of enzyme-inhibitor interactions were studied through molecular modeling technology. Furthermore, the druggability of chalcone-rivastigmine hybrids was evaluated using *in silico* ADMET prediction and SH-SY5Y cell line assay.

2. Materials and methods

2.1. Chemistry

The high-resolution mass spectra were generated on an Bruker Agilent1290 /maXis mass spectrometer with an ESI mass selective detector. NMR spectra were recorded using TMS as the internal standard on a Bruker Avance III spectrometer at 400 (^{1}H NMR) and 101 or 151 (^{13}C NMR) MHz. Melting points were determined on an Stuart-smp40 Melt automated melting point instrument. The reactions were followed by thin-layer chromatography (TLC) on glass-packed precoated silica gel plates and visualized with a UV lamp. Flash column chromatography was performed using silica gel (200–300 mesh) purchased from Qingdao Haiyang Chemical Co. Ltd. The purity ($\geq$ 95%) of the synthesized compounds was determined by HPLC (Table S1).

2.2. General procedure for the synthesis of intermediate compounds (M1-M14)

A suspension of ketone or aldehyde (0.044 mol), K_2CO_3/1.5H_2O (0.785 eq, 0.035 mol) and K_2CO_3 (0.215 eq, 0.009 mol) in appropriate ethyl acetate was added pyridine (0.144 eq, 0.006 mol). The mixture was stirred and heated to 70 ℃. Acyl chloride (1.5

eq, 0.066 mol) in appropriate ethyl acetate was added dropwise. The reaction was stirred at 70 ºC, and was monitored by TLC. Upon completion, an equal volume of water was added to the mixture, stirred at 70 ºC for 1.5 h. The reaction was cooled and the aqueous layer was separately washed 2x with 2% H_2SO_4 and water, then the combined organics were dried over $MgSO_4$, filtered, and concentrated in vacuo to provide the target products (**M1-M14,** Yield: 85%-98%).

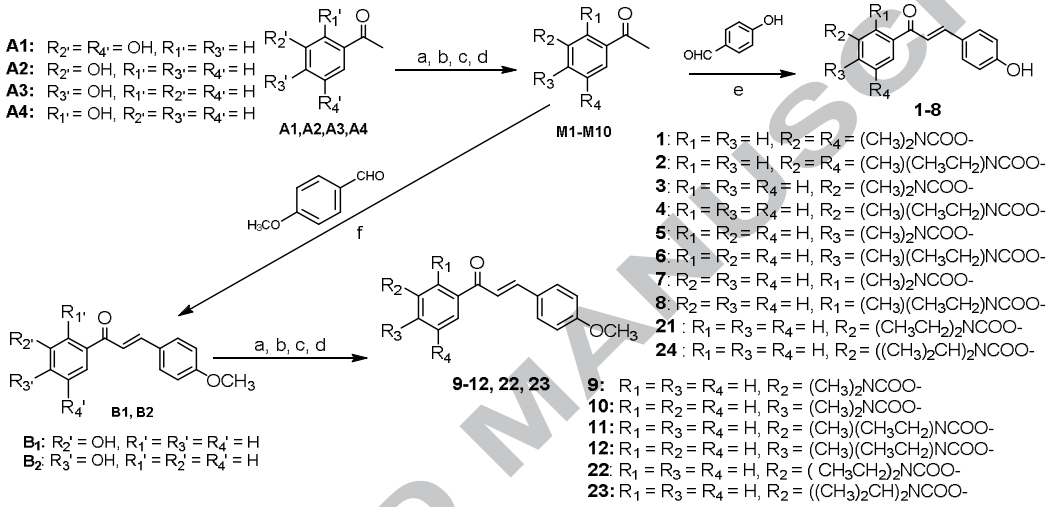

Scheme 1. Synthesis of compounds **1-8**, **9-12**, **21-24**. Reagents and conditions: (a) N,N-Dimethylcarbamoyl chloride (b) N-Ethyl-N-methylcarbamoyl Chloride (c) Diethylcarbamyl Chloride (d) Diisopropylcarbamyl chloride, K_2CO_3, $K_2CO_3/1.5H_2O$, Pyridine, ethyl acetate, 70 ºC, 12-36 h; (e) 37% HCl, ethyl alcohol, 70 ºC,24-36 h; (f) 8% KOH, CH_3OH, 70 ºC, 24-36 h.

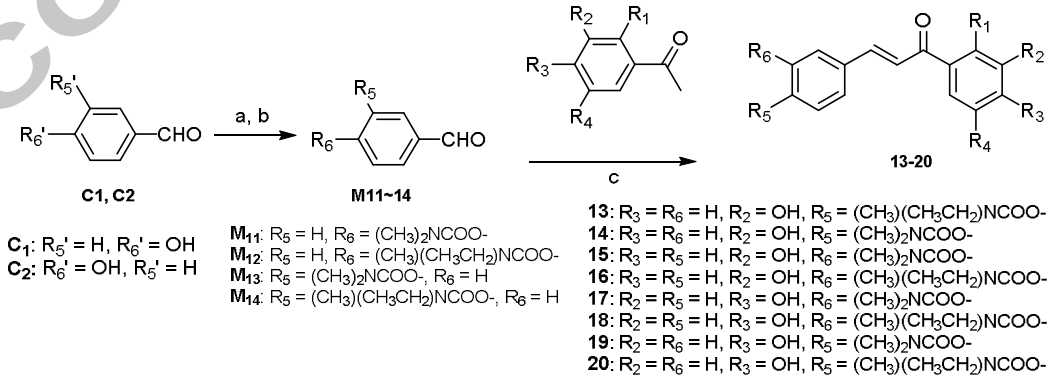

Scheme 2. Synthesis of compounds **13-20**. Reagents and conditions: (a) N,N-

Dimethylcarbamoyl chloride (b) N-Ethyl-N-methylcarbamoyl Chloride, K_2CO_3, $K_2CO_3/1.5H_2O$, pyridine, ethyl acetate, H_2O, 70 ºC, 12-36 h; (c) 37% HCl, ethyl alcohol, 70 ºC, 24-36 h.

2.3. General procedure for the synthesis of B1 and B2

M4 or **M6** (2 mmol) was dissolved in 5 mL methanol, 4 mL 8% KOH solution was added dropwise at room temperature. P-anisaldehyde in appropriate methanol was added to the mixture slowly. The reaction was stirred at room temperature for 72 h. After the completion of the reaction, excess solvent was evaporated in vacuo. Then the solution was partitioned between 90 mL water and 90 mL methylene chloride. The organic layer was washed 3x with water, and the combined organics were dried over $MgSO_4$, filtered, and concentrated in vacuo to provide a crude product which was purified by flash column chromatography on silica gel (eluent: Ethyl acetate/petroleum) to afford the desired product.

2.3.1. (*E*)-1-(3-hydroxyphenyl)-3-(4-methoxyphenyl)prop-2-en-1-one (B1)

Pale yellow solid, 45.9% Yield. M.P. 126.5–128.3 ºC. ^{1}H NMR (400 MHz, DMSO-d_6) δ 9.76 (s, 1H), 7.84 (d, J = 8.7 Hz, 2H), 7.70 (s, 2H), 7.60 (d, J = 7.7 Hz, 1H), 7.44 (s, 1H), 7.36 (t, J = 7.9 Hz, 1H), 7.08-6.97 (m, 3H), 3.83 (s, 3H). ^{13}C NMR (101 MHz, DMSO-d_6) δ 189.42, 161.81, 158.16, 144.30, 139.76, 131.23, 130.25, 127.77, 120.52, 120.14, 119.93, 115.02, 114.88, 55.84. HRMS: calcd for $C_{16}H_{14}O_3$, $[M + Na]^+$, *m/z* 277.0835; found, *m/z* 277.0835; HPLC purity: 95.44%.

2.3.2. (*E*)-1-(4-hydroxyphenyl)-3-(4-methoxyphenyl)prop-2-en-1-one (B2)

Pale yellow solid, 35.4% Yield. M.P. 181.5–183.4 ºC. ^{1}H NMR (400 MHz, DMSO-d_6) δ 10.35 (s, 1H), 8.05 (d, J = 8.7 Hz, 2H), 7.82 (d, J = 8.7 Hz, 2H), 7.77 (d, J = 15.5 Hz, 1H), 7.65 (d, J = 15.5 Hz, 1H), 7.01 (d, J = 8.8 Hz, 2H), 6.89 (d, J = 8.7 Hz, 2H), 3.82 (s, 3H). ^{13}C NMR (101 MHz, DMSO-d_6) δ 187.50, 162.48, 161.58, 143.16, 131.51, 131.01, 129.81, 127.99, 120.02, 115.79, 114.82, 55.80. HRMS: calcd for $C_{16}H_{14}O_3$, $[M + Na]^+$, *m/z* 277.0835; found, *m/z* 277.0836; HPLC purity: 98.04%.

2.4. General procedure for the synthesis of compound 1-8

M1~M8 (2 mmol) and p-hydroxybenzaldehyde (2.4 mmol) was dissolved in 10 mL ethanol, 10 drops concentrated hydrochloric acid was added dropwise at room temperature. The reaction was stirred at room temperature. The reaction was monitored by TLC. After the completion of the reaction, excess solvent was evaporated in vacuo. Then the solution was partitioned between 90 mL water and 90 mL methylene chloride. The organic layer was dried over $MgSO_4$, filtered, and concentrated in vacuo to provide a crude product which was purified by flash column chromatography on silica gel (eluent: Ethyl acetate/petroleum) to afford the desired product.

2.4.1. (*E*)-5-(3-(4-hydroxyphenyl)acryloyl)-1,3-phenylene-bis(dimethylcarbamate) (1)

Yellow solid, 12.8% Yield. M.P. 170–172 ℃. ^{1}H NMR (400 MHz, DMSO-d_6) δ 10.12 (s, 1H), 7.78 (d, J = 8.7 Hz, 2H), 7.76 (d, J = 2.2 Hz, 2H), 7.72 (s, 2H), 7.26 (s, 1H), 6.84 (d, J = 8.6 Hz, 2H), 3.01 (d, J = 56.5 Hz, 12H). ^{13}C NMR (101 MHz, DMSO-d_6) δ 187.90, 161.05, 154.05, 152.28, 145.97, 139.64, 131.79, 126.29, 120.66, 118.63, 117.97, 116.14, 36.92, 36.50. HRMS: calcd for $C_{21}H_{22}N_2O_6$, $[M + H]^+$, m/z 399.1551; found, m/z 399.1555; HPLC purity: 98.98%.

2.4.2. (*E*)-5-(3-(4-hydroxyphenyl)acryloyl)-1,3-phenylene-bis(ethyl(methyl)-carbamate) (2)

Yellow solid, 22.9% Yield. M.P. 150–152 ℃. ^{1}H NMR (400 MHz, DMSO-d_6) δ 10.14 (s, 1H), 7.77 (dd, J = 15.3, 9.2 Hz, 6H), 7.27 (t, J = 2.1 Hz, 1H), 6.85 (d, J = 8.6 Hz, 2H), 3.46 (dd, J = 13.8, 6.8 Hz, 2H), 3.37–3.30 (m, 2H), 2.99 (d, J = 52.8 Hz, 6H), 1.22 (t, J = 7.0 Hz, 3H), 1.12 (t, J = 7.0 Hz, 3H). ^{13}C NMR (101 MHz, DMSO-d_6) δ 187.72, 160.83, 157.75, 153.68, 152.34, 145.84, 139.89, 131.79, 129.79, 126.17, 120.89, 119.07, 118.38, 116.26, 115.67, 44.04, 34.42, 34.07, 13.52, 12.71. HRMS:

calcd for $C_{23}H_{26}N_2O_6$, $[M + H]^+$, *m/z* 427.1864; found, *m/z* 427.1864; HPLC purity: 97.76%.

2.4.3. (*E*)-3-(3-(4-hydroxyphenyl)acryloyl)phenyl dimethylcarbamate (3)

Yellow solid, 9% Yield. M.P. 153–155 ℃. ^{1}H NMR (400 MHz, DMSO-d_6) δ 10.10 (s, 1H), 7.99 (d, J = 7.9 Hz, 1H), 7.88–7.84 (m, 1H), 7.76 (d, J = 8.7 Hz, 2H), 7.71 (d, J = 1.1 Hz, 2H), 7.57 (t, J = 7.9 Hz, 1H), 7.41 (ddd, J = 8.0, 2.3, 0.9 Hz, 1H), 6.84 (d, J = 8.6 Hz, 2H), 3.08 (d, J = 9.3 Hz, 3H), 2.93 (d, J = 4.2 Hz, 3H). ^{13}C NMR (101 MHz, DMSO-d_6) δ 188.48, 160.73, 154.36, 152.10, 145.41, 139.61, 131.64, 130.09, 126.91, 126.20, 125.59, 122.18, 118.69, 116.28, 36.81, 36.61. HRMS: calcd for $C_{18}H_{17}NO_4$, $[M + H]^+$, *m/z* 312.1230; found, *m/z* 312.1235; HPLC purity: 99.63%.

2.4.4. (*E*)-3-(3-(4-hydroxyphenyl)acryloyl)phenyl ethyl(methyl)carbamate (4)

Pale yellow solid, 12.8% Yield. M.P. 118.9–121.5 ℃. ^{1}H NMR (400 MHz, DMSO-d_6) δ 10.10 (s, 1H), 7.99 (d, J = 7.7 Hz, 1H), 7.84 (s, 1H), 7.76 (d, J = 8.5 Hz, 2H), 7.71 (s, 2H), 7.57 (t, J = 7.9 Hz, 1H), 7.41 (d, J = 7.9 Hz, 1H), 6.84 (d, J = 8.5 Hz, 2H), 3.47 (d, J = 6.8 Hz, 1H), 2.99 (d, J = 56.4 Hz, 3H), 1.26–1.09 (m, 4H). ^{13}C NMR (101 MHz, DMSO-d_6) δ 188.31, 160.79, 153.92, 152.06, 145.41, 139.62, 132.95, 131.64, 130.08, 126.89, 126.19, 125.59, 122.11, 118.69, 116.28, 44.00, 34.40, 34.07, 13.55, 12.73. HRMS: calcd for $C_{19}H_{19}NO_4$, $[M + Na]^+$, *m/z* 348.1206; found, *m/z* 348.1213; HPLC purity: 99.87%.

2.4.5. (*E*)-4-(3-(4-hydroxyphenyl)acryloyl)phenyl dimethylcarbamate (5)

Yellow solid, 30% Yield. M.P. 188.5–170.3 ℃. ^{1}H NMR (400 MHz, DMSO-d_6) δ 10.10 (s, 1H), 8.17 (d, J = 8.6 Hz, 2H), 7.76 (d, J = 3.3 Hz, 4H), 7.73 (d, J = 3.3 Hz, 2H), 7.70 (s, 1H), 7.29 (t, J = 8.7 Hz, 2H), 6.86 (t, J = 12.1 Hz, 2H), 3.07 (s, 3H), 2.94 (s, 3H). ^{13}C NMR (101 MHz, DMSO-d_6) δ 188.26, 160.61, 155.29, 153.87, 144.91, 135.27, 131.48, 130.29, 126.25, 122.39, 118.83, 116.28, 36.81, 36.63. HRMS: calcd for $C_{18}H_{17}NO_4$, $[M + Na]^+$, 334.1055; found, *m/z* 334.1053; HPLC purity: 99.83%.

2.4.6. (*E*)-4-(3-(4-hydroxyphenyl)acryloyl)phenyl ethyl(methyl)carbamate (6)

Yellow solid, 59.7% Yield. M.P. 145.9–146.5 ºC. ^{1}H NMR (400 MHz, DMSO-d_6) δ 10.10 (s, 1H), 8.17 (d, J = 8.6 Hz, 2H), 7.76 (d, J = 2.8 Hz, 4H), 7.73 (d, J = 4.0 Hz, 2H), 7.68 (d, J = 15.5 Hz, 1H), 7.30 (d, J = 8.5 Hz, 2H), 6.84 (d, J = 8.6 Hz, 2H), 3.50–3.34 (m, 2H), 2.99 (d, J = 50.0 Hz, 3H), 1.23–1.09 (m, 3H). ^{13}C NMR (101 MHz, DMSO-d_6) δ 188.30, 160.61, 155.28, 153.40, 144.92, 135.25, 131.48, 130.29, 126.25, 122.38, 118.82, 116.28, 44.04, 34.41, 34.11, 13.53, 12.69. HRMS: calcd for $C_{19}H_{19}NO_4$, $[M + H]^+$, *m/z* 326.1387; found, *m/z* 326.1388; HPLC purity: 98.37%.

2.4.7. (*E*)-2-(3-(4-hydroxyphenyl)acryloyl)phenyl dimethylcarbamate (7)

Yellow liquid, 11.1% Yield. ^{1}H NMR (400 MHz, DMSO-d_6) δ 10.13 (s, 1H), 7.66 (dd, J = 7.6, 1.6 Hz, 1H), 7.58 (dd, J = 10.7, 5.0 Hz, 3H), 7.47–7.32 (m, 2H), 7.23 (s, 1H), 7.11 (d, J = 15.9 Hz, 1H), 6.82 (d, J = 8.6 Hz, 2H), 2.92 (s, 3H), 2.77 (s, 3H). ^{13}C NMR (101 MHz, DMSO-d_6) δ 191.34, 160.78, 157.77, 153.97, 149.48, 145.05, 131.15, 129.80, 125.99, 125.78, 124.19, 122.63, 119.23, 116.37, 36.70, 36.45. HRMS: calcd for $C_{18}H_{17}NO_4$, $[M + Na]^+$, *m/z* 334.1050; found, *m/z* 334.1055; HPLC purity: 99.91%.

2.4.8. (*E*)-2-(3-(4-hydroxyphenyl)acryloyl)phenyl ethyl(methyl)carbamate (8)

Pale yellow solid, 15.7% Yield. M.P. 109.5–111.6 ºC. ^{1}H NMR (400 MHz, DMSO-d_6) δ 10.12 (s, 1H), 7.64 (t, J = 7.6 Hz, 1H), 7.58 (d, J = 8.1 Hz, 3H), 7.43 (d, J = 15.9 Hz, 1H), 7.36 (t, J = 7.3 Hz, 1H), 7.24 (d, J = 8.0 Hz, 1H), 7.09 (dd, J = 15.9, 8.9 Hz, 1H), 6.82 (d, J = 8.6 Hz, 2H), 3.34–3.28 (m, 1H), 3.17 (q, J = 7.0 Hz, 1H), 2.84 (d, J = 47.8 Hz, 3H), 0.98 (dt, J = 55.8, 7.0 Hz, 3H). ^{13}C NMR (151 MHz, DMSO-d_6) δ 191.23, 160.70, 153.50, 149.49, 145.18, 145.02, 133.66, 132.60, 131.18, 129.83, 125.97, 124.09, 122.57, 116.27, 43.81, 34.24, 33.94, 13.28, 12.50. HRMS: calcd for $C_{19}H_{19}NO_4$, $[M + Na]^+$, *m/z* 348.1206; found, *m/z* 348.1207; HPLC purity: 99.92%.

2.5. General procedure for the synthesis of compound 9-12, 22, and 23

A suspension of B1 or B2 (0.47 mmol), $K_2CO_3/1.5H_2O$ (0.369 mmol) and K_2CO_3 (0.101 mmol) in appropriate ethyl acetate was added 4 drops pyridine. The mixture was stirred and heated to 70 ℃. Acyl chloride (0.705 mmol) in appropriate ethyl acetate was added dropwise. Then the reaction was stirred at 70 ℃, the reaction was monitored by TLC. Upon completion, an equal volume of water was added to the mixture, stirred at 70 ℃ for 1.5 h. The reaction was cooled and the aqueous layer was separately washed 2x with 2% H_2SO_4 and water, then the combined organics were dried over $MgSO_4$, filtered, and concentrated in vacuo to give the desired product.

2.5.1. (*E*)-3-(3-(4-methoxyphenyl)acryloyl)phenyl dimethylcarbamate (9)

Pale yellow solid, 98% Yield. M.P. 60–62 ℃. ^{1}H NMR (400 MHz, DMSO-d_6) δ 8.01 (d, J = 7.8 Hz, 1H), 7.87 (t, J = 11.6 Hz, 3H), 7.81–7.70 (m, 2H), 7.58 (t, J = 7.9 Hz, 1H), 7.42 (dd, J = 8.0, 1.5 Hz, 1H), 7.03 (d, J = 8.7 Hz, 2H), 3.83 (s, 3H), 3.09 (s, 3H), 2.94 (s, 3H). ^{13}C NMR (101 MHz, DMSO-d_6) δ 188.57, 161.99, 154.35, 152.12, 144.92, 139.48, 131.42, 130.11, 127.72, 127.03, 125.67, 122.23, 119.74, 114.86, 55.85, 36.81, 36.60. HRMS: calcd for $C_{19}H_{19}NO_4$, $[M + H]^+$, *m/z* 326.1387; found, *m/z* 326.1387; HPLC purity: 97.81%.

2.5.2. (*E*)-4-(3-(4-methoxyphenyl)acryloyl)phenyl dimethylcarbamate (10)

Pale yellow solid, 72.4% Yield. M.P. 110.2–112.1 ℃. ^{1}H NMR (400 MHz, DMSO-d_6) δ 8.19 (d, J = 8.6 Hz, 2H), 7.85 (dd, J = 9.7, 6.1 Hz, 4H), 7.83–7.79 (m, 0H), 7.74 (t, J = 9.7 Hz, 0H), 7.31 (d, J = 8.6 Hz, 2H), 7.02 (t, J = 7.2 Hz, 2H), 3.83 (d, J = 2.9 Hz, 3H), 3.07 (s, 3H), 2.94 (s, 3H). ^{13}C NMR (101 MHz, DMSO-d_6) δ 188.30, 161.85, 155.38, 153.86, 144.42, 135.15, 131.28, 130.37, 127.78, 122.42, 119.88, 114.87, 55.85, 36.81, 36.64. HRMS: calcd for $C_{19}H_{19}NO_4$, $[M + Na]^+$, *m/z* 348.1206; found, *m/z* 348.1206; HPLC purity: 97.03%.

2.5.3. (*E*)-3-(3-(4-methoxyphenyl)acryloyl)phenyl ethyl(methyl)carbamate (11)

Yellow liquid, 81.5% Yield. ^{1}H NMR (400 MHz, DMSO-d_6) δ 8.01 (d, J = 7.8 Hz, 1H), 7.87 (t, J = 11.3 Hz, 5H), 7.80 (s, 0H), 7.75 (d, J = 15.5 Hz, 0H), 7.58 (t, J = 7.9

Hz, 1H), 7.42 (d, *J* = 8.0 Hz, 1H), 7.03 (d, *J* = 8.7 Hz, 2H), 3.83 (s, 3H), 3.53–3.34 (m, 1H), 3.00 (d, *J* = 56.7 Hz, 3H), 1.23–1.11 (m, 4H). ^{13}C NMR (101 MHz, DMSO-d_6) δ 188.57, 161.94, 153.89, 152.08, 144.92, 139.49, 131.43, 130.12, 127.72, 127.07, 125.68, 122.17, 119.75, 114.87, 55.86, 44.00, 34.41, 34.07, 13.54, 12.73. HRMS: calcd for $C_{20}H_{21}NO_4$, $[M + Na]^+$, *m/z* 362.1363; found, *m/z* 362.1365; HPLC purity: 95.99%.

2.5.4. (*E*)-4-(3-(4-methoxyphenyl)acryloyl)phenyl ethyl(methyl)carbamate (12)

Yellow liquid, 81.5% Yield. ^{1}H NMR (400 MHz, DMSO-d_6) δ 8.19 (d, *J* = 8.7 Hz, 2H), 7.90–7.83 (m, 2H), 7.81 (s, 1H), 7.73 (d, *J* = 15.5 Hz, 1H), 7.30 (t, *J* = 9.6 Hz, 2H), 7.03 (d, *J* = 8.8 Hz, 2H), 3.52–3.40 (m, 1H), 3.35 (d, *J* = 7.1 Hz, 1H), 3.06–2.90 (m, 3H), 1.23–1.10 (m, 3H). ^{13}C NMR (101 MHz, DMSO-d_6) δ 188.30, 161.85, 155.36, 153.51, 144.43, 135.14, 131.28, 130.38, 127.79, 122.41, 119.88, 114.87, 55.84, 44.04, 34.41, 34.11, 13.53, 12.69. HRMS: calcd for $C_{20}H_{21}NO_4$, $[M + H]^+$, *m/z* 340.1543; found, *m/z* 340.1548; HPLC purity: 95.47%.

2.5.5. (*E*)-3-(3-(4-methoxyphenyl)acryloyl)phenyl diethylcarbamate (22)

Yellow liquid, 67% Yield. ^{1}H NMR (400 MHz, DMSO-d_6) δ 8.03 (d, *J* = 7.7 Hz, 1H), 7.89 (d, *J* = 8.6 Hz, 5H), 7.85 (s, 0H), 7.81 (s, 0H), 7.76 (d, *J* = 15.5 Hz, 0H), 7.58 (t, *J* = 7.9 Hz, 1H), 7.43 (d, *J* = 7.9 Hz, 1H), 7.03 (d, *J* = 8.6 Hz, 2H), 3.84 (s, 3H), 3.45 (dd, *J* = 13.1, 6.2 Hz, 2H), 3.26 (dd, *J* = 16.2, 7.5 Hz, 2H), 1.25 (d, *J* = 6.9 Hz, 6H), 1.14 (t, *J* = 7.1 Hz, 1H). ^{13}C NMR (151 MHz, DMSO-d_6) δ 188.61, 161.97, 153.65, 152.08, 144.95, 139.52, 131.45, 130.14, 127.74, 127.07, 125.71, 122.12, 119.77, 114.88, 55.87, 42.24, 13.54. HRMS: calcd for $C_{21}H_{23}NO_4$, $[M + H]^+$, *m/z* 354.1700; found, *m/z* 354.1700; HPLC purity: 96.00%.

2.5.6. (*E*)-3-(3-(4-methoxyphenyl)acryloyl)phenyl diisopropylcarbamate (23)

Brown liquid, 91.7% Yield. ^{1}H NMR (400 MHz, DMSO-d_6) δ 8.04 (d, *J* = 7.8 Hz, 1H), 7.89 (d, *J* = 8.8 Hz, 5H), 7.83 (d, *J* = 15.5 Hz, 2H), 7.76 (d, *J* = 15.5 Hz, 1H), 7.58 (t, *J* = 7.9 Hz, 1H), 7.40 (dd, *J* = 8.0, 1.6 Hz, 1H), 7.03 (d, *J* = 8.8 Hz, 2H), 4.03

(dt, J = 13.3, 6.8 Hz, 2H), 3.83 (s, 3H), 1.28 (d, J = 20.4 Hz, 14H). ^{13}C NMR (101 MHz, DMSO-d_6) δ 188.68, 161.97, 153.05, 151.96, 144.95, 139.55, 131.46, 130.15, 127.73, 127.03, 125.66, 121.93, 119.82, 114.89, 55.87, 46.76, 21.76, 20.65. HRMS: calcd for $C_{23}H_{27}NO_4$, $[M + H]^+$, m/z 382.2013; found, m/z 382.2011; HPLC purity: 95.12%.

2.6. General procedure for the synthesis of 21 and 24

M9 or **M10** (4 mmol) and p-hydroxybenzaldehyde (4 mmol) was dissolved in 20 mL ethanol, 15 drops concentrated hydrochloric acid was dropwised at room temperature. The reaction was stirred at room temperature. The reaction was monitored by TLC, after the completion of the reaction, excess solvent was evaporated in vacuo. Then the solution was partitioned between 105 mL ethyl acetate and 180 mL water. The organic layer was washed 2x with water, and the combined organics were dried over $MgSO_4$, filtered, and concentrated in vacuo to provide a crude product which was purified by flash column chromatography on silica gel (eluent: Ethyl acetate/petroleum) to afford the desired product.

2.6.1. (*E*)-3-(3-(4-hydroxyphenyl)acryloyl)phenyl diethylcarbamate (21)

Brown solid, 16% Yield. M.P. 110.5–111.9 ºC. ^{1}H NMR (400 MHz, DMSO-d_6) δ 10.13 (s, 1H), 8.01 (d, J = 7.8 Hz, 1H), 7.84 (s, 1H), 7.74 (dd, J = 23.9, 12.5 Hz, 4H), 7.63–7.53 (m, 1H), 7.41 (dd, J = 8.0, 1.7 Hz, 1H), 6.85 (d, J = 8.5 Hz, 2H), 3.45 (dd, J = 13.3, 6.4 Hz, 2H), 3.33 (dd, J = 13.9, 6.9 Hz, 2H), 1.23 (dd, J = 15.1, 8.4 Hz, 3H), 1.15 (dd, J = 14.8, 7.9 Hz, 3H). ^{13}C NMR (101 MHz, DMSO-d_6) δ 188.56, 160.76, 153.66, 152.06, 145.44, 139.65, 131.67, 130.11, 126.95, 126.22, 125.62, 122.07, 118.73, 116.30, 42.25, 42.00, 14.67, 13.74. HRMS: calcd for $C_{20}H_{21}NO_4$, $[M + H]^+$, m/z 340.1543; found, m/z 340.1546; HPLC purity: 98.37%.

2.6.2. (*E*)-3-(3-(4-hydroxyphenyl)acryloyl)phenyl diisopropylcarbamate (24)

Yellow solid, 7.8% Yield. M.P. 153.1–155.1 ºC. ^{1}H NMR (400 MHz, DMSO-d_6) δ 10.14 (s, 1H), 8.02 (d, J = 7.8 Hz, 1H), 7.74 (dd, J = 24.2, 12.6 Hz, 5H), 7.63–7.49 (m,

1H), 7.39 (dd, *J* = 8.0, 1.6 Hz, 1H), 6.85 (d, *J* = 8.6 Hz, 2H), 4.01 (dq, *J* = 13.3, 6.6 Hz, 2H), 1.25 (t, *J* = 21.9 Hz, 13H). ^{13}C NMR (101 MHz, DMSO-d_6) δ 188.63, 160.76, 153.06, 151.95, 145.45, 139.67, 131.68, 130.13, 126.92, 126.20, 125.58, 121.88, 118.75, 116.30, 46.75, 21.72, 20.60. HRMS: calcd for $C_{22}H_{25}NO_4$, $[M + H]^+$, *m/z* 368.1856; found, *m/z* 368.1860; HPLC purity: 99.34%.

2.7. General procedure for the synthesis of 13-20

M11~M14 (4 mmol) and 3'-Hydroxyacetophenone or 4'-Hydroxyacetophenone (4mmol) was dissolved in 20 mL ethanol, 20 drops concentrated hydrochloric acid was added dropwise at room temperature. The reaction was stirred at room temperature. The reaction was monitored by TLC, after the completion of the reaction, excess solvent was evaporated in vacuo. Then the solution was partitioned between 100 mL water and 150 mL ethyl acetate. The organic layer was dried over $MgSO_4$, filtered, and concentrated in vacuo to provide a crude product which was purified by flash column chromatography on silica gel (eluent: Ethyl acetate/petroleum) to afford the desired product.

2.7.1. (*E*)-4-(3-(3-hydroxyphenyl)-3-oxoprop-1-en-1-yl)phenyl ethyl(methyl) carbamate (13)

Yellow-green solid, 9% Yield. M.P. 117.9–199.6 ℃. ^{1}H NMR (400 MHz, DMSO-d_6) δ 9.82 (d, *J* = 9.3 Hz, 1H), 7.91 (d, *J* = 8.6 Hz, 2H), 7.83 (d, *J* = 15.6 Hz, 1H), 7.72 (d, *J* = 15.6 Hz, 1H), 7.64 (d, *J* = 7.7 Hz, 1H), 7.46 (d, *J* = 1.9 Hz, 1H), 7.38 (t, *J* = 7.9 Hz, 1H), 7.21 (d, *J* = 8.4 Hz, 2H), 7.06 (dd, *J* = 7.9, 2.2 Hz, 1H), 3.44 (dd, *J* = 14.1, 7.0 Hz, 1H), 3.31 (d, *J* = 7.0 Hz, 1H), 2.97 (d, *J* = 49.5 Hz, 3H), 1.23–1.08 (m, 3H). ^{13}C NMR (101 MHz, DMSO-d_6) δ 189.01, 157.71, 153.25, 152.99, 142.96, 139.01, 131.61, 129.90, 129.79, 122.28, 121.89, 120.24, 119.54, 114.60, 43.50, 33.89, 33.57, 13.03, 12.21. HRMS: calcd for $C_{19}H_{19}NO_4$, $[M + H]^+$, *m/z* 326.1387; found, *m/z* 326.1390; HPLC purity: 96.48%.

2.7.2. (*E*)-4-(3-(3-hydroxyphenyl)-3-oxoprop-1-en-1-yl)phenyl dimethyl

carbamate (14)

Yellow solid, 9% Yield. M.P. 144.2–146.1 ℃. ^{1}H NMR (400 MHz, DMSO-d_6) δ 9.80 (s, 1H), 7.88 (s, 1H), 7.70 (d, J = 15.9 Hz, 4H), 7.48 (s, 2H), 7.38 (t, J = 7.9 Hz, 1H), 7.21 (dd, J = 7.8, 2.0 Hz, 1H), 7.07 (dd, J = 8.1, 2.4 Hz, 1H), 3.09 (s, 3H), 2.94 (s, 3H). ^{13}C NMR (101 MHz, DMSO-d_6) δ 189.48, 158.21, 154.12, 153.49, 143.48, 139.49, 132.14, 130.43, 130.31, 122.81, 122.36, 120.76, 120.07, 115.08, 36.79, 36.61. HRMS: calcd for $C_{18}H_{17}NO_4$, $[M + Na]^+$, *m/z* 334.1050; found, *m/z* 334.1056; HPLC purity: 98.14%.

2.7.3. (*E*)-3-(3-(3-hydroxyphenyl)-3-oxoprop-1-en-1-yl)phenyl dimethyl carbamate (15)

Yellow liquid, 9% Yield. ^{1}H NMR (400 MHz, DMSO-d_6) δ 9.83 (s, 1H), 7.90 (d, J = 15.6 Hz, 1H), 7.71 (d, J = 16.2 Hz, 4H), 7.48 (s, 2H), 7.38 (t, J = 7.9 Hz, 1H), 7.21 (d, J = 7.8 Hz, 1H), 7.11–7.02 (m, 1H), 3.54–3.37 (m, 2H), 2.99 (d, J = 54.8 Hz, 3H), 1.23–1.12 (m, 4H). ^{13}C NMR (101 MHz, DMSO-d_6) δ 189.52, 158.22, 154.43, 152.28, 143.31, 139.37, 136.54, 130.31, 130.17, 126.78, 124.66, 123.49, 121.96, 120.86, 120.15, 115.15, 36.81, 36.61. HRMS: calcd for $C_{18}H_{17}NO_4$, $[M + Na]^+$, *m/z* 334.1050; found, *m/z* 334.1056; HPLC purity: 97.42%.

2.7.4. (*E*)-3-(3-(3-hydroxyphenyl)-3-oxoprop-1-en-1-yl)phenylethyl-(methyl) carbamate (16)

Yellow solid, 7.6% Yield. M.P. 90.1–91.9 ℃. ^{1}H NMR (400 MHz, DMSO-d_6) δ 9.81 (s, 1H), 7.91 (d, J = 8.6 Hz, 2H), 7.84 (d, J = 15.6 Hz, 1H), 7.72 (d, J = 15.6 Hz, 1H), 7.64 (d, J = 7.7 Hz, 1H), 7.49–7.45 (m, 1H), 7.38 (t, J = 7.9 Hz, 1H), 7.22 (d, J = 8.6 Hz, 2H), 7.08–7.05 (m, 1H), 3.06 (s, 4H), 2.92 (d, J = 8.1 Hz, 4H). ^{13}C NMR (101 MHz, DMSO-d_6) δ 189.48, 158.22, 153.96, 152.22, 143.36, 139.34, 136.53, 130.32, 130.17, 126.85, 124.70, 123.41, 122.00, 120.87, 120.19, 115.13, 43.97, 34.39, 34.06, 13.55, 12.76. HRMS: calcd for $C_{19}H_{19}NO_4$, $[M + Na]^+$, *m/z* 348.1206; found, *m/z* 348.1206; HPLC purity: 97.18%.

2.7.5. (*E*)-3-(3-(4-hydroxyphenyl)-3-oxoprop-1-en-1-yl)phenyl dimethyl carbamate (17)

Yellow-green solid, 12.8% Yield. M.P. 164.7–166.5 ºC. ^{1}H NMR (400 MHz, DMSO-d_6) δ 10.44 (s, 1H), 8.10 (d, J = 8.7 Hz, 2H), 7.95 (d, J = 15.6 Hz, 1H), 7.71 (d, J = 14.0 Hz, 2H), 7.45 (t, J = 7.9 Hz, 1H), 7.19 (d, J = 5.6 Hz, 1H), 6.90 (d, J = 8.6 Hz, 2H), 3.08 (s, 3H), 2.94 (s, 3H). ^{13}C NMR (101 MHz, DMSO-d_6) δ 187.46, 162.76, 154.45, 152.24, 142.25, 136.75, 131.77, 130.13, 129.49, 126.75, 124.45, 123.32, 121.80, 115.85, 36.78, 36.59. HRMS: calcd for $C_{18}H_{17}NO_4$, $[M + Na]^+$, *m/z* 334.1050; found, *m/z* 334.1055; HPLC purity: 97.39%.

2.7.6. (*E*)-3-(3-(4-hydroxyphenyl)-3-oxoprop-1-en-1-yl)phenyl-ethyl(methyl) carbamate (18)

Pale green solid, 8.3% Yield. M.P. 149.5–151.3 ºC. ^{1}H NMR (400 MHz, DMSO-d_6) δ 10.43 (s, 1H), 8.10 (d, J = 8.7 Hz, 2H), 7.95 (d, J = 15.6 Hz, 1H), 7.74–7.64 (m, 3H), 7.45 (t, J = 7.9 Hz, 1H), 7.19 (d, J = 7.6 Hz, 1H), 6.90 (d, J = 8.7 Hz, 2H), 3.46 (d, J = 7.2 Hz, 1H), 3.35 (s, 1H), 3.07–2.90 (m, 3H), 1.13 (t, J = 7.1 Hz, 3H). ^{13}C NMR (101 MHz, DMSO-d_6) δ 187.48, 162.76, 154.09, 152.21, 142.27, 136.76, 131.77, 130.13, 129.49, 126.73, 124.51, 123.32, 121.81, 115.85, 43.97, 34.38, 34.06, 13.56, 12.76. HRMS: calcd for $C_{19}H_{19}NO_4$, $[M + Na]^+$, *m/z* 348.1206; found, *m/z* 348.1209; HPLC purity: 96.53%.

2.7.7. (*E*)-4-(3-(4-hydroxyphenyl)-3-oxoprop-1-en-1-yl)phenyl-dimethyl carbamate (19)

Pale green solid, 23% Yield. M.P. 154.2–155.8 ºC. ^{1}H NMR (400 MHz, DMSO-d_6) δ 10.43 (s, 1H), 8.09 (d, J = 8.6 Hz, 2H), 7.98–7.82 (m, 3H), 7.69 (d, J = 15.6 Hz, 1H), 7.21 (d, J = 8.5 Hz, 2H), 6.91 (d, J = 8.6 Hz, 2H), 3.06 (s, 3H), 2.93 (s, 3H). ^{13}C NMR (101 MHz, DMSO-d_6) δ 187.87, 162.66, 154.15, 153.29, 142.35, 132.36, 131.64, 130.22, 129.67, 122.75, 122.33, 115.85, 36.80, 36.61. HRMS: calcd for $C_{18}H_{17}NO_4$, $[M + Na]^+$, *m/z* 334.1050; found, *m/z* 334.1053; HPLC purity: 98.54%.

2.7.8. (*E*)-4-(3-(4-hydroxyphenyl)-3-oxoprop-1-en-1-yl)phenyl-ethyl(methyl) carbamate (20)

Yellow-green solid, 14.9% Yield. M.P. 150.5–152.0 ºC. ^{1}H NMR (400 MHz, DMSO-d_6) δ 10.43 (s, 1H), 8.07 (t, J = 13.0 Hz, 2H), 7.88 (dd, J = 15.6, 10.6 Hz, 3H), 7.69 (d, J = 15.5 Hz, 1H), 7.21 (d, J = 8.1 Hz, 2H), 7.06–6.82 (m, 2H), 3.63–3.14 (m, 3H), 2.95 (dd, J = 46.9, 17.1 Hz, 3H), 1.30–0.96 (m, 4H). ^{13}C NMR (101 MHz, DMSO-d_6) δ 187.54, 162.66, 153.90, 153.28, 142.36, 132.35, 131.64, 130.22, 129.63, 122.75, 122.32, 115.85, 34.40, 34.09, 13.54, 12.73. HRMS: calcd for $C_{19}H_{19}NO_4$, [M + Na]$^+$, *m/z* 348.1206; found, *m/z* 348.1209; HPLC purity: 98.57%.

2.8. Biology

2.8.1. *In vitro* inhibition of hAChE and hBChE

Acetylcholinesterase (from human recombinant, C1682,), butyrylcholinesterase (from human serum, B4186), 5,5'-dithiobis (2-nitrobenzoic acid) (DTNB, D8130), acetylthiocholine iodide (ATC, A5751,), and S-Butyrylthiocholine iodide (BTC, B3253) were purchased from Sigma Chemical Co.

Ellman assay was employed to measure the inhibition effect of designed compounds on hAChE and hBChE activity.[26] Compounds were diluted with reaction buffer (phosphate buffer, 0.08 M Na_2HPO_4 and 0.02 M NaH_2PO_4, pH 8.0). 0.004 U/mL hAChE or 0.002 U/mL hBChE was incubated with each compound at 37 ºC for 15 min. Then 5,5'-dithiobis (2-nitrobenzoic acid) was added to a final concentration of 50 μM. After mixing with ATC for hAChE, or BTC for hBChE at a final concentration of 50 μM, the complex was scanned immediately at 412 nm using Thermo Scientific Varioskan Flash. The average absorbance variation for 5 consecutive minutes was calculated. The inhibitory rate for each compound was calculated by comparing the average absorbance of samples containing compounds with that absence of test compound. The dose-response curve and concentration needed to inhibit 50% enzyme activity (IC_{50}) was calculated in Graph Pad version 6.01 by fitting replicates with the log (inhibitor) vs normalized response variable slope equation.

2.8.2. Kinetic characterization of hAChE and hBChE inhibition

The kinetic studies of compound **3** against hAChE and hBChE were performed. After incubating 0.004 U/mL hAChE or 0.002 U/mL hBChE with diluted compound at three concentrations range from 100 nM to 900 nM at 37 ℃ for 15 min. Then DTNB was added as usual, and substrate was added finally with six serial diluted concentrations range from 0.125 mM to 1 mM. Enzyme activities were determined immediately at 412 nm using Thermo Scientific Varioskan Flash for five minutes at one min interval. Kinetic characterizations of the hydrolysis of substrate by hAChE and hBChE were analyzed by estimating kinetic parameters K_m, V_{max} in Michaelis-Menten plot in Graph Pad. Then the data were plotted on a Lineweaver–Burk diagram to reveal the mechanism of inhibition.

2.8.3. *In vitro* cell viability assay

Cytotoxicity was measured with an MTT (3-(4,5-dimethyl-2-thiazolyl)-2,5-diph enyl-2-H-tetrazolium bromide) assay protocol.[27, 28] 5×10^3 SH-SY5Y cells were seeded in a 96-well plate with 100 μL of culture medium. After incubation f or 16-18 hours, the culture medium were changed to 100 μL indicated medium in the presence of compounds at the concentration of 6.25 μM, 12.5 μM, 25 μM, 50 μM and 100 μM, respectively. After incubation for 48 hours, the cells were further incubated with 20 μL of 2.5 mg/mL MTT for 4 hours at 37 ℃ in a humidified incubator with 5% CO_2. After dissolution of the formazan dy e in 120 μL of DMSO was added to the cells, and the absorbance was measu red at 490 nm by using EnSpire-2300 Multimode Reader (PerkinElmer).

2.8.4. Antioxidation activity assay

Intracellular ROS was stimulated by tert-Butyl hydroperoxide (t-BHP) and measured with the fluorescent probe (2',7'-dichlorofluorescein diacetate (DCFH-DA).[28] For assays, SH-SY5Y cells were cultured in 24-well plates at a seeding density of 5×104 cells per well. After 16-18 h, the cells were treated with

compound **3** and curcumin. After 24 h of treatment with the compounds, the cells were washed with PBS and then incubated with 5 μM DCFH-DA and 100 μM t-BHP in PBS at 37 ºC in 5% CO2 for 30 min. After the cells were washed with PBS and resuspended, the fluorescence of the cells from each well was measured at 488 nm excitation, and 525 nm emission, with a Flow Cytometer (CytoFLEX, Beckman Coulter). Results are expressed as a percentage of the sample average divided by the control group data, calculated as follows: (FIsample-FIblank) / (FIcontrol-FIblank) × 100%.

2.9. Molecular modeling

2.9.1. Molecular docking

The crystal structures of the hAChE (PDB ID: 4EY7)[29] and hBChE (PDB ID: 4TPK)[30] were derived from the RCSB Protein Data Bank. The resolution of hAChE and hBChE structures was 2.35 and 2.7 Å, respectively. The structures of compound **3**, donepezil, and 3F9 were drawn using ISIS draw and optimized based on MMFF94 force field using MOE 2010.10 (Chemical Computing Group Inc.).[31] Two protein structures were preprocessed (i.e., protonated, removed water, and then minimized with the CHARMm force field, etc.) with the "Protein Preparation Protocol" in the Discovery Studio 3.5 (DS 3.5, Accelrys Inc.). The native ligand in the crystal structure was used to define the binding site. The docking program CDOCKER encoded in DS 3.5 was applied to identify the potential binding of compound **3** to the hAChE and hBChE. Other CDOCKER parameters were set to default values. During the docking process, 20 poses were retained. After running CDOCKER, the poses were visually inspected, and the most suitable docking pose was selected on the basis of the score and interactions with key residues of the active site of hAChE and hBChE. The complexes of hAChE and hBChE and compound **3** acquired from the docking experiments were used as the initial coordinates for the subsequent molecular dynamics (MD) simulations.

2.9.2. Molecular dynamics simulations

The proteins were assigned with the AMBER ff99SB force field[32] Parameters for compound **3** were obtained from the ANTECHAMBER module using the Generalized Amber Force Field (GAFF)[33] with the RESP charge-fitting procedure with input from HF/6-31G* calculations made with the Gaussian 09 package.[34] All hydrogen atoms of the protein were added using the tleap module, considering ionizable residues set at their default protonation states at a neutral pH. The systems were solvated in a TIP3P water box with a minimum distance of 10 Å between any protein atom and the edge of the box. 20 ns MD simulations were performed in AMBER 12 and the processes of MD simulations were taken from our previously studies.[34-36] After MD simulation, 100 snapshots were extracted from the last 2 ns of the trajectory at intervals of 15 ps. The MM-GBSA method in the AMBER 12 suite was used to calculate the binding free energies.[37, 38]

2.9.3. *In silico* pharmacokinetic properties of the active compounds

ADME/T properties, including the absorption, solubility, BBB, hepatotoxicity, CYP 2D6, alogP, and PSA of the 13 actives, have been evaluated *in silico* through DS 3.5.

3. Results and discussion

3.1. Chemistry

A series of chalcone-rivastigmine hybrids were prepared by using previously published methods.[39-41] The synthetic routes for the target compounds are listed in Schemes 1 and 2. Various corresponding hydroxyphenylcetone (**A1**, **A2**, **A3**, and **A4**) or hydroxy benzaldehyde (**C1** and **C2**) were first acylated by reacting with carbamoylchloride in the presence of K_2CO_3, $K_2CO_3/1.5H_2O$, and catalyst pyridine to afford the intermediate compounds (**M1~M14**), then the target compounds were obtained from **M1**-**M14** by using Claisene-Schmidt condensation.

As shown in Scheme 1, **M1~M10** reacted with p-hydroxy benzaldehyde to provide the target compounds **1**-**8**, **21**, and **24**. **M4** and **M6** reacted with p-methoxybenzaldehyde to generate **B1** and **B2**, which was further acylated to afford the target compounds **9**-**12**, **22**, and **23**. Target compounds **13**-**20** were synthesized

with **M11~M14**, corresponding hydroxyphenylacetone by the same aldol condensation procedure (Scheme 2).

3.2. Inhibition of hAChE and hBChE

All targeted compounds were evaluated *in vitro* for their inhibition of hBChE and hAChE using Ellman assay.[26] The results are depicted in Supplementary Figure S1. The 13 of 26 compounds showed > 50% inhibition activity against hBChE at 10 μM. The IC_{50} values of the 13 active compounds were further characterized (Table 1 and Figure S2). Rivastigmine was used as a positive control with an IC_{50} value of 0.38 μM. Compound **3** is the most potent inhibitor of hBChE with an IC_{50} of 0.36 μM, which is comparable or slightly better than that of rivastigmine.

Analyzing the SAR, it is well established that several structural elements determine the hBChE inhibitory activity of chalcone-rivastigmine hybrids as follows: (i) the introduction of 3-substituted carbamate in A ring could increase inhibitory activity against hBChE, while 4- or 5-substituted carbamate will lose or decrease the activity (**1**, **2**, **5**, **6**, **11**, and **12**, Table 1); (ii) the 5- or 6-substituted carbamate in B ring will keep the activity against hBChE (**15**-**18**); (iii) simultaneously 3- and 5-substituted carbamates in A ring of chalcone will lose the inhibitory activity (**1**-**2**); and (iv) the alkyl substituent on the carbamoyl nitrogen strongly affects the affinity profile (dimethyl > bis(ethyl(methyl)) > diethyl), and the most potent inhibitors were methyl derivatives (**3**, **9**, **15**, **17**, and **19**). Moreover, compared with **9** and **11**, compounds **B1** and **B2** (not chalcone-rivastigmine hybrids analogues) did not exhibit inhibition against hBChE, demonstrating that carbamate in our designed compounds is necessary for hBChE.

The results at hAChE had a potency trend dissimilar to that observed at hBChE. Only 3-substituted dimethylcarbamate in A ring of chalcone exhibited inhibitory activity against hAChE (**3** and **9**). The bis(ethyl(methyl) carbamate and diethyl carbamate derivatives will lose the potency, which are good in agreement with previous studies. Similar with hBChE, simultaneously 3- and 5-substituted carbamates in A ring of chalcone lost the inhibitory activity against hAChE (**1**-**2**). The

most potent hAChE inhibitor is compound **3** with an IC_{50} of 0.872 μM, which is approximately 3-fold better than that of rivastigmine.

Consequently, similar with rivastigmine, the new compound **3** with a dual inhibitory action on both hAChE and hBChE might show a better therapeutic profile in AD and related dementia.[19]

Table 1. Inhibitory activity of compounds against hAChE and hBChE.

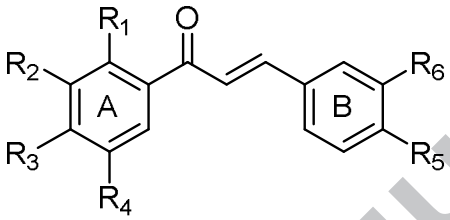

Compounds	R_1	R_2	R_3	R_4	R_5	R_6	IC_{50} (μM)[a]	
							hAChE	hBChE
1	—H	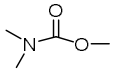	—H	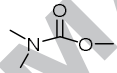	—OH	—H	ND	ND
2	—H	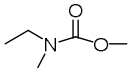	—H	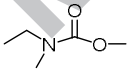	—OH	—H	ND	ND
3	—H	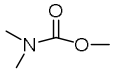	—H	—H	—OH	—H	0.87±0.19	0.36±0.01
4	—H	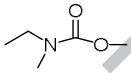	—H	—H	—OH	—H	ND	4.37±0.38
5	—H	—H	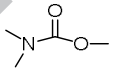	—H	—OH	—H	ND	ND
6	—H	—H	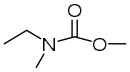	—H	—OH	—H	ND	ND
7	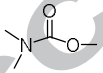	—H	—H	—H	—OH	—H	ND	ND
8		—H	—H	—H	—OH	—H	ND	5.97±0.08
9	—H	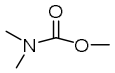	—H	—H	—OCH_3	—H	8.05±0.54	3.37±0.50
10	—H	—H	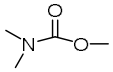	—H	—OCH_3	—H	ND	ND
11	—H	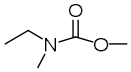	—H	—H	—OCH_3	—H	ND	3.93±0.56

12	—H	—H	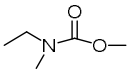	—H	—OCH_3	—H	ND	7.36±0.98
13	—H	—OH	—H	—H	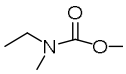	—H	ND	5.60±0.37
14	—H	—OH	—H	—H	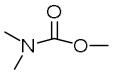	—H	ND	ND
15	—H	—OH	—H	—H	—H	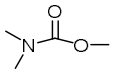	ND	1.91±0.27
16	—H	—OH	—H	—H	—H	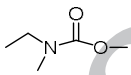	ND	2.87±0.19
17	—H	—H	—OH	—H	—H	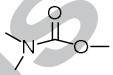	ND	2.19±0.55
18	—H	—H	—OH	—H	—H	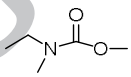	ND	2.52±0.54
19	—H	—H	—OH	—H	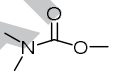	—H	ND	4.48±0.50
20	—H	—H	—OH	—H	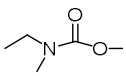	—H	ND	6.08±0.78
21	—H	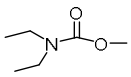	—H	—H	—OH	—H	ND	ND
22	—H	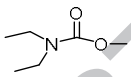	—H	—H	—OCH_3	—H	ND	ND
23	—H	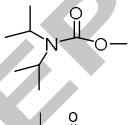	—H	—H	—OCH_3	—H	ND	ND
24	—H		—H	—H	—OH	—H	ND	ND
B1	—H	—OH	—H	—H	—OCH_3	—H	ND	ND
B2	—H	—H	—OH	—H	—OCH_3	—H	ND	ND
Rivastigmine *b*							3.12±0.46	0.38±0.02

[a] IC_{50} values are indicated as the mean±SD (standard error) of three independent experiments. [b] Rivastigmine: a positive control compound. ND: not determined (because the inhibitory activities were too weak to permit an IC_{50} determination).

3.3. Kinetic evaluation of compound 3

To obtain the mechanism of hAChE and hBChE inhibition, kinetic experiments were performed. As shown in Figure 2A and 2C, the lines intersect at the negative x-axis into a same point, and V_{max} decreases as the concentration of compound **3** increases. The Lineweaver–Burk plots suggest that **3** is a typically non-competitive for hAChE and hBChE. The mechanism of action was also confirmed by plotting substrate-velocity curves in the presence of several concentrations of compound **3** (Figure 2B and 2D). The kinetic constant (K_i) of hAChE and hBChE were estimated to be 0.52 ± 0.04 and 0.16 ± 0.01 μM.

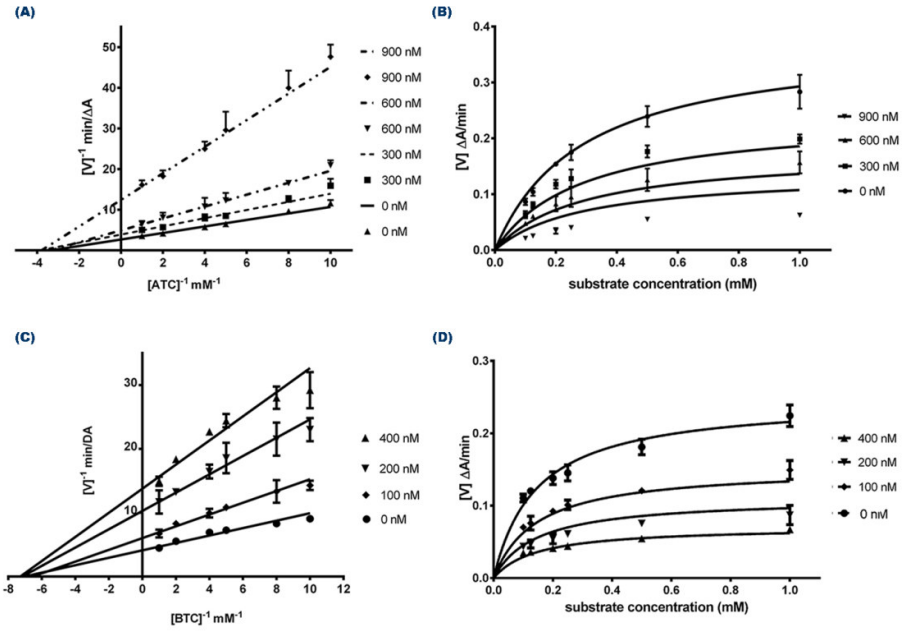

Figure 2. Kinetic studies on the mechanism of hAChE and hBChE inhibition by compound **3**. Overlaid Lineweaver–Burk reciprocal plots of the hAChE (A) and hBChE (C) initial velocity at increasing substrate in the absence and presence of compound **3**. Substrate-velocity plots in the presence of several concentrations of compound **3** (B) for hAChE and (D) for hBChE.

3.5. Characteristic binding patterns of compound 3

The binding modes of compound **3** with hAChE and hBChE were investigated by molecular docking. The native ligands, donepezil and 3F9, were redocked back to the binding sites of hAChE and hBChE , and the root-mean-square deviations (RMSD) of

the redocked and native ligand poses were 0.39 and 0.46 Å (Figure S3), indicating that CDOCKER was a capable docking method for our complex systems. The docking scores of compound **3** with hAChE and hBChE are –26.7 and –36.4 kcal/mol, respectively. Subsequently, the stability and energy profile of the docking poses of compound **3** were investigated through MD simulations and the calculations of binding free energies. Figure 3A shows the time dependence of the RMSD values for structure backbone atoms of two enzymes and compound **3** over the production phase of simulation. The RMSD values of simulation converged after ~2 ns, indicating that the system is stable and equilibrated. The RMSD values of ligand compared docking pose is swinging within 0.75 Å, illustrating that the docking pose is reliable.

The detailed binding modes of compound **3** and hAChE and hBChE were revealed from the conformation clustering analysis. As shown in Figure 3B and 3C, the carbamate ester of compound **3** inserted the catalytic triad of hAChE (SER203 and HIS447) and hBChE (SER198 and HIS438). Similar with rivastigmine, this binding direction of the carbamate ester will be hydrolyzed, resulting in hAChE and hBChE inhibition.[18, 42] Compared with hBChE, the compound **3** was surrounded with big and hydrophobic side chains of the binding pocket of hAChE (e.g., PHE338, PHE295, PHE297, TRP86, and TRP286, Figure 3B), suggesting that steric hindrance is not negatively affected during lead optimizations. The observed results from the binding pockets of hAChE and hBChE are consistent with our SAR analysis results. For hBChE, compound **3** can form two hydrogen bonds with the side chains of GLY117 and THR120 (Figure 3C). Superimposition of compound **3** and hAChE and hBChE suggests that compound **3** occupies the catalytic binding pocket in a pattern similar to that of rivastigmine (Figure 3D).[18]

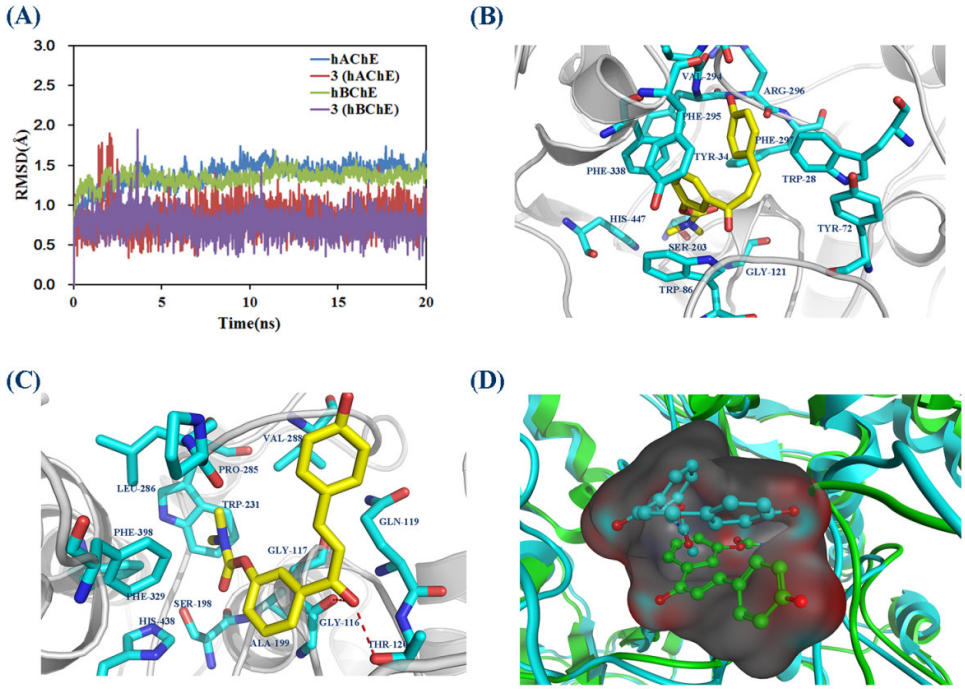

Figure 3. Stability properties of the simulation systems and binding model of compound **3** with hAChE and hBChE. (A) RMSD plots for the backbone atoms and compound **3** during 20 ns MD simulations; the detailed bind modes of compound **3** with (B) hAChE and (C) hBChE; (D) superposition of compound **3** in the binding pockets of hAChE (cyan) and hBChE (green). Hydrogen bonds are shown by red dashed lines. The cutoff value for the formation of a hydrogen bond is 3.5 Å.

The MM-GBSA method was used to calculate the binding free energies and to gain information on the different components of interaction energy that contribute to compound **3** binding for hAChE and hBChE. Detailed results are shown in Table 2. Table 2 indicates that van der Waals (ΔE_{vdw}) and electrostatic components (ΔE_{ele}) play key roles in compound **3** binding for both hAChE and hBChE. The van der Waals contribution is approximately 1.6- and 1.7-fold greater than the electrostatic component for hAChE and hBChE, respectively. Non-polar component to solvation ($\Delta E_{nonpol,solv}$) values are also favorable for compound **3** binding (e.g., –5.42 kcal/molfor hAChE and –8.38 kcal/mol for hBChE), while polar component to solvation ($\Delta E_{pol,solv}$) does not favor compound **3** binding (Table 2). The binding free energy of compound **3**-hBChE is higher than that of compound **3**-hAChE, which is

consistent with our bioassay results (Table 1).

Table 2. Binding free energy for compound **3** based on MM-GBSA method.

Energy terms	Binding free energy (Kcal/mol) (SEM)	
	compound **3**-hAChE	compound **3**-hBChE
ΔE_{vdw} [a]	–40.99 (4.95)	–38.33 (4.23)
ΔE_{ele} [b]	–25.60 (4.81)	–22.68 (3.79)
$\Delta E_{pol,solv}$ [c]	37.26 (4.64)	29.82 (3.49)
$\Delta E_{nonpol,solv}$ [d]	–5.42 (0.58)	–8.38 (0.31)
ΔG_{gas} [e]	–66.59 (8.06)	–57.01 (7.28)
ΔG_{solv} [f]	31.84 (4.20)	24.43 (2.97)
ΔG_{bind} [g]	–34.75 (5.03)	–36.57 (5.17)

[a]Non-bonded van der Waals; [b]Non-bonded electrostatics; [c]Polar component to solvation; [d]Non-polar component to solvation; [e]Total gas phase energy; [f]Sum of nonpolar and polar contributions to solvation; [g]Final estimated binding free energy calculated from the terms above. Standard errors of the mean are given in parentheses.

Energy decomposition analysis was conducted to identification of key residues contributing to binding affinity. Generally, if the interaction energy between the residue and the ligand is lower than –1 kcal/mol, those residues are considered to be hot residues.[2, 27] As shown in Figure 4, the hot residues of hAChE are TRP86, TYR124, VAL294, PHE338, and TYR341, while the hot residues of hBChE are TRP82, GLY116, GLY17, SER198, TRP231 TYR332, and PHE329. The hot residues from decomposition results are consistent with the binding mode analyses (Figure 3B and 3C), which provides a theoretical basis for further lead optimization.

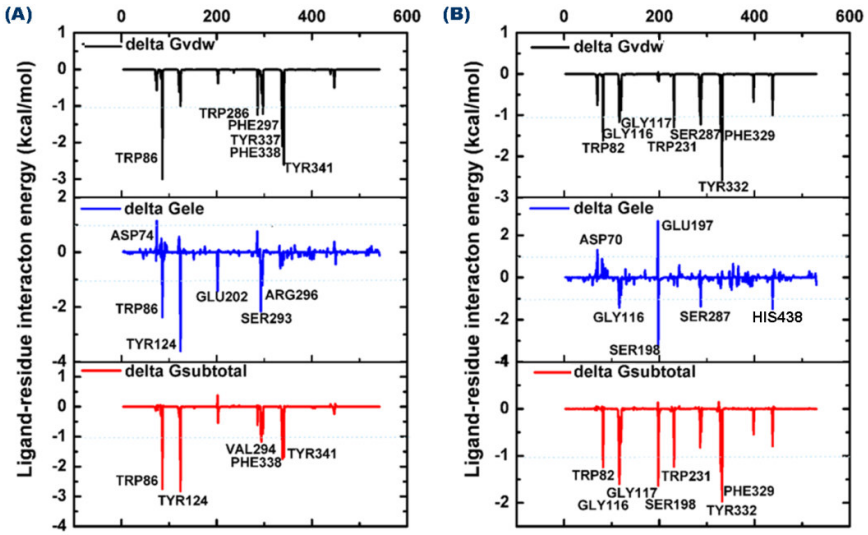

Figure 4. Ligand−residue interaction energies from MM-GBSA energy decomposition for compound **3**-hAChE (A) and compound **3**-hBChE (B). Delta Gsubtotal represents total estimated binding free energy for each residue. Delta Gele represents non-bonded electrostatics interactions. Delta Gvdw represents non-bonded van der Waals interactions.

3.6. Cell viability assay on the SH-SY5Y cell Line

A preliminary toxicity of the 13 chalcone-rivastigmine hybrids was assessed using cell viability assays on the SH-SY5Y cell line. The results are listed in Supplementary Table S2. The most active compound 3 exhibited 96.66% and 94.62% cell viability at 12.5 and 25 μM, suggesting that compound 3 did not significantly reduce cell viability. In general, the cell toxicity profile of compound 3 roughly matches that of rivastigmine, with higher cytotoxicity at the highest tested concentration (50 and 100 μM, Figure 5). Compared to the drug rivastigmine, the similar potency, lack of toxicity, and new chemotype of compound **3** suggests that it is worthy of further development.

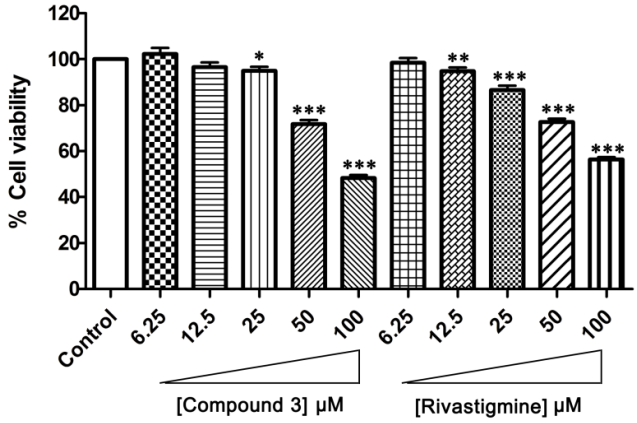

Figure 5. Cell viability in SH-SY5Y cells for compound **3** and rivastigmine. Data correspond to the mean ± SEM of different experiments performed in triplicate. *$p <$ 0.05, **$p < 0.01$, and ***$p < 0.001$ versus control.

3.7. Compound 3 reduces the production of oxidative stress in SH-SY5Y cell lines

SH-SY5Y cells were incubated with compound **3** in 5 µM and 1 µM concentrations. The cells were also incubated with curcumin (a known antioxidant) in the same concentration series. Figure 6 shows that the ROS is significantly inhibited by compound **3** (1 and 5 µM, respectively), which is superior to curcumin in the same concentration.

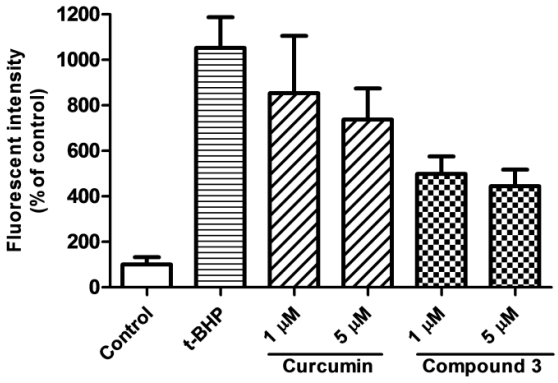

Figure 6. Compound **3** inhibits ROS in SH-SY5Y cell lines. The results are represented in the percentage of control cells. The untreated cells were used as negative control, and curcumin was used as a positive control.

3.8. *In silico* ADME/T properties of active compounds

The ADME/T properties of 13 hBChE inhibitors were assessed using DS 3.5. Compared with rivastigmine, most of these inhibitors satisfied ADMET rules defined in ADMET module of DS 3.5, especially for compound **3**. The detailed results and comparisons can be found in Table 3. As shown in Table 3, compound **3** may cross the blood-brain barrier (BBB). Moreover, active compounds don't contain problematic substructures suggested from Pan Assay Interference Compounds (PAINS).[43] All of these results suggested that the compound **3** designed in the present study provided a valuable alternative for AD and related dementia treatment.

Table 3. *In silico* predicted ADMET properties of the 13 compounds.[a]

Compounds	Absorption[b]	Solubility[c]	BBB[d]	CYP2D6[e]	Hepatotoxic[f]	AlogP98[g]	PSA[h]
3	0	-3.763	-0.165	-4.182	-3.025	3.429	67.699
4	0	-3.972	-0.058	-5.317	-3.174	3.778	67.699
8	0	-4.009	-0.058	-5.016	-2.444	3.778	67.699
9	0	-4.257	0.092	-6.217	-3.381	3.655	55.814
11	0	-4.459	0.200	-6.346	-3.875	4.003	55.814
12	0	-4.417	0.200	-6.333	-2.891	4.003	55.814
13	0	-3.929	-0.058	-5.619	-3.070	3.778	67.699
15	0	-3.758	-0.165	-3.811	-2.520	3.429	67.699
16	0	-3.966	-0.058	-4.946	-2.669	3.778	67.699
17	0	-3.758	-0.165	-3.509	-2.335	3.429	67.699
18	0	-3.966	-0.058	-4.645	-2.484	3.778	67.699
19	0	-3.726	-0.165	-4.168	-2.041	3.429	67.699
20	0	-3.929	-0.058	-5.304	-2.191	3.778	67.699
Rivastigmine[i]	0	-3.171	0.128	-2.499	-1.324	2.599	32.935

[a]ADMET properties were calculated using DS 3.5. [b]Predicted human intestinal absorption level (0: Good absorption; 1: Moderate absorption; 2: Low absorption; 3: Very low absorption). [c]Predicted aqueous solubility level (< -8.0: Extremely low; -8.0 to -6.0: No, very low, but possible; -6.0 to -4.0: Yes, low; -4.0 to -2.0: Yes, good; -2.0 to 0.0: Yes, optimal; 0.0 < : No, too soluble). [d]Predicted Blood brain barrier (BBB, ≥ 0.7: Very high penetrant; 0 to 0.7: High penetrant; -0.52 to 0: Medium penetrant; ≤ -0.52: Low penetrant). [e]Predicted cytochrome P450 2D6 enzyme inhibition (CYP2D6, < 0.162: Non-inhibitor; ≥ 0.162: Inhibitor). [f]Predicted hepatotoxicity (< -0.409: Nontoxic; ≥ -0.409: Toxic). [g]AlogP98: Atom-based LogP. [h]PSA: Fast polar surface area. [i]Rivastigmine: a positive control compound.

4. Conclusion

In conclusion, a novel series of chalcone-rivastigmine hybrids were designed,

synthesized, and evaluated *in vitro* for their ability to inhibit hAChE and hBChE. Biological assays demonstrated that compound **3** is a dual hAChE and hBChE inhibitor with IC_{50} values (0.87 and 0.36 μM), which are comparable or slightly better than that of the commercially available drug, rivastigmine. The detailed mechanisms of enzyme-**3** interactions at atomic level were investigated using kinetic experiments, molecular docking, molecular dynamics simulations, and binding free energies analyses. Compared with rivastigmine, cell viability assay on the SH-SY5Y cell line showed compound **3** has negligible toxicity. Furthermore, compound **3** can blocks the formation of reactive oxygen species (ROS) in SH-SY5Y cells and is in the required druggability ranges from *in silico* ADMET prediction. Thus, compound **3** is worthy of further development and the further *in vivo* study of compound **3** is in progress.

Acknowledgment

This work was funded in part by the Science and Technology Planning Project of Guangdong Province (No. 2015B010109004), the Natural Science Foundation of Guangdong Province (No. 2016A030310421), the National Natural Science Foundation of China (No. 81502984, 81373395, and 81573415), the Fundamental Research Funds for the Central Universities (No. 2015ZM049), the China Postdoctoral Science Foundation (No. 2015M572325), the Shanghai Municipal Science and Technology Commission (No. 14431905600), Guangdong Provincial Key Laboratory of Construction Foundation (No. 2011A060901014), the Open Project Program of Guangdong Key Laboratory of Fermentation and Enzyme Engineering, SCUT (FJ2015006).

References

1. Ballard, C.; Gauthier, S.; Corbett, A.; Brayne, C.; Aarsland, D.; Jones, E. *Lancet* **2011,** *377*, 1019.
2. Wang, L.; Zeng, R. R.; Pang, X. Q.; Gu, Q.; Tan, W. *RSC Adv.* **2015,** *5*, 66391.
3. Sinha, S.; Lieberburg, I. *P. Natl Acad. Sci. USA.* **1999,** *96*, 11049.
4. Brus, B.; Kosak, U.; Turk, S.; Pislar, A.; Coquelle, N.; Kos, J.; Stojan, J.; Colletier, J. P.; Gobec, S. *J. Med. Chem.* **2014,** *57*, 8167.
5. Francis, P. T.; Palmer, A. M.; Snape, M.; Wilcock, G. K. *J. Neurol. Neurosurg. Psychiatry* **1999,** *66*, 137.
6. Bartus, R. T.; Dean, R. L., 3rd; Beer, B.; Lippa, A. S. *Science* **1982,** *217*, 408.
7. Tago, H.; Maeda, T.; McGeer, P. L.; Kimura, H. *J. Comp. Neurol.* **1992,** *325*, 301.

8. Ballard, C. G.; Greig, N. H.; Guillozet-Bongaarts, A. L.; Enz, A.; Darvesh, S. *Curr. Alzheimer Res.* **2005,** *2*, 307.
9. Giacobini, E. *Pharmacol. Res.* **2004,** *50*, 433.
10. Zemek, F.; Drtinova, L.; Nepovimova, E.; Sepsova, V.; Korabecny, J.; Klimes, J.; Kuca, K. *Expert Opin. Drug Saf.* **2014,** *13*, 759.
11. Shinagawa, S.; Shigeta, M. *Brain. Nerve.* **2014,** *66*, 507.
12. Li, B.; Duysen, E. G.; Carlson, M.; Lockridge, O. *J. Pharmacol. Exp. Ther.* **2008,** *324*, 1146.
13. Mesulam, M. M.; Guillozet, A.; Shaw, P.; Levey, A.; Duysen, E. G.; Lockridge, O. *Neuroscience* **2002,** *110*, 627.
14. Holmes, C.; Ballard, C.; Lehmann, D.; Smith, A. D.; Beaumont, H.; Day, I. N.; Khan, M. N.; Lovestone, S.; McCulley, M.; Morris, C. M.; Munoz, D. G.; O'Brien, K.; Russ, C.; Del Ser, T.; Warden, D. *J. Neurol. Neurosur. Ps.* **2005,** *76*, 640.
15. Greig, N. H.; Utsuki, T.; Ingram, D. K.; Wang, Y.; Pepeu, G.; Scali, C.; Yu, Q. S.; Mamczarz, J.; Holloway, H. W.; Giordano, T.; Chen, D. M.; Furukawa, K.; Sambamurti, K.; Brossi, A.; Lahiri, D. K. *P. Natl. Acad. Sci. USA.* **2005,** *102*, 17213.
16. Gottwald, M. D.; Rozanski, R. I. *Expert Opin. Investig. Drugs* **1999,** *8*, 1673.
17. Bullock, R. *Int. J. Clin. Pract.* **2002,** *56*, 206.
18. Bolognesi, M. L.; Bartolini, M.; Cavalli, A.; Andrisano, V.; Rosini, M.; Minarini, A.; Melchiorre, C. *J. Med. Chem.* **2004,** *47*, 5945.
19. Giacobini, E.; Spiegel, R.; Enz, A.; Veroff, A. E.; Cutler, N. R. *J. Neural. Transm.* **2002,** *109*, 1053.
20. Carolan, C. G.; Dillon, G. P.; Gaynor, J. M.; Reidy, S.; Ryder, S. A.; Khan, D.; Marquez, J. F.; Gilmer, J. F. *J. Med. Chem.* **2008,** *51*, 6400.
21. Go, M. L.; Wu, X.; Liu, X. L. *Curr. Med. Chem.* **2005,** *12*, 481.
22. Chen, J.; Yan, J.; Hu, J. H.; Pang, Y. Q.; Huang, L.; Li, X. S. *RSC Adv.* **2015,** *5*, 68128.
23. Chimenti, F.; Fioravanti, R.; Bolasco, A.; Chimenti, P.; Secci, D.; Rossi, F.; Yanez, M.; Orallo, F.; Ortuso, F.; Alcaro, S. *J. Med. Chem.* **2009,** *52*, 2818.
24. Lahtchev, K. L.; Batovska, D. I.; Parushev, S. P.; Ubiyvovk, V. M.; Sibirny, A. A. *Eur. J. Med. Chem.* **2008,** *43*, 2220.
25. Chen, Y. P.; Zhang, Z. Y.; Li, Y. P.; Li, D.; Huang, S. L.; Gu, L. Q.; Xu, J.; Huang, Z. S. *Eur. J. Med. Chem.* **2013,** *66*, 22.
26. Ellman, G. L.; Courtney, K. D.; Andres, V., Jr.; Feather-Stone, R. M. *Biochem. Pharmacol.* **1961,** *7*, 88.
27. Wang, L.; Chen, L.; Yu, M.; Xu, L. H.; Cheng, B.; Lin, Y. S.; Gu, Q.; He, X. H.; Xu, J. *Sci. Rep-Uk.* **2016,** *6*.
28. Cao, Y. Y.; Wang, L.; Ge, H.; Lu, X. L.; Pei, Z.; Gu, Q.; Xu, J. *Mol. Divers.* **2013,** *17*, 515.
29. Cheung, J.; Rudolph, M. J.; Burshteyn, F.; Cassidy, M. S.; Gary, E. N.; Love, J.; Franklin, M. C.; Height, J. J. *J. Med. Chem.* **2012,** *55*, 10282.
30. Brus, B.; Kosak, U.; Turk, S.; Pislar, A.; Coquelle, N.; Kos, J.; Stojan, J.; Colletier, J. P.; Gobec, S. *J. Med. Chem.* **2014,** *57*, 8167.
31. Cheng, A.; Best, S. A.; Merz, K. M.; Reynolds, C. H. *J. Mol. Graph. Model.* **2000,** *18*, 273.
32. Hornak, V.; Abel, R.; Okur, A.; Strockbine, B.; Roitberg, A.; Simmerling, C. *Proteins* **2006,** *65*, 712.
33. Zhang, W.; Hou, T. J.; Qiao, X. B.; Xu, X. J. *J. Phys. Chem. B.* **2003,** *107*, 9071.
34. Cui, L.; Wang, Y.; Liu, Z. H.; Chen, H. Z.; Wang, H.; Zhou, X. X.; Xu, J. *J. Chem. Inf. Model.* **2015,**

55, 2455.
35. Xu, B.; Wang, L.; Gonzalez-Molleda, L.; Wang, Y.; Xu, J.; Yuan, Y. *Antimicrob. Agents Ch.* **2014,** *58*, 563.
36. Wang, L.; Gu, Q.; Zheng, X. H.; Ye, J. M.; Liu, Z. H.; Li, J. B.; Hu, X. P.; Hagler, A.; Xu, J. *J. Chem. Inf. Model.* **2013,** *53*, 2409.
37. Miller, B. R.; McGee, T. D.; Swails, J. M.; Homeyer, N.; Gohlke, H.; Roitberg, A. E. *J. Chem. Theory Comput.* **2012,** *8*, 3314.
38. Kollman, P. A.; Massova, I.; Reyes, C.; Kuhn, B.; Huo, S. H.; Chong, L.; Lee, M.; Lee, T.; Duan, Y.; Wang, W.; Donini, O.; Cieplak, P.; Srinivasan, J.; Case, D. A.; Cheatham, T. E. *Accounts Chem. Res.* **2000,** *33*, 889.
39. Cao, G.; Hu, A. X.; Zou, K. S.; Xu, L.; Chen, J. L.; Tan, W. *Chirality* **2008,** *20*, 856.
40. Bois, F.; Boumendjel, A.; Mariotte, A. M.; Conseil, G.; Di Petro, A. *Bioorgan. Med. Chem.* **1999,** *7*, 2691.
41. Satyanarayana, M.; Tiwari, P.; Tripathi, B. K.; Srivastava, A. K.; Pratap, R. *Bioorgan. Med. Chem.* **2004,** *12*, 883.
42. Baron, P.; Millard, C. B.; Harel, M.; Dvir, H.; Enz, A.; Sussman, J. L.; Silman, I. *Biochemistry* **2002,** *41*, 3555.
43. Baell, J. B.; Holloway, G. A. *J. Med. Chem.* **2010,** *53*, 2719.

Figure captions

Figure 1. Chemical structures of ChE ligands and chalcone.

Figure 2. Kinetic studies on the mechanism of hAChE and hBChE inhibition by compound **3**. Overlaid Lineweaver–Burk reciprocal plots of the hAChE (A) and hBChE (C) initial velocity at increasing substrate in the absence and presence of compound **3**. Substrate-velocity plots in the presence of several concentrations of compound **3** (B) for hAChE and (D) for hBChE.

Figure 3. Stability properties of the simulation systems and binding model of compound **3** with hAChE and hBChE. (A) RMSD plots for the backbone atoms and compound **3** during 20 ns MD simulations; the detailed bind modes of compound **3** with (B) hAChE and (C) hBChE; (D) superposition of compound **3** in the binding pockets of hAChE (cyan) and hBChE (green). Hydrogen bonds are shown by red dashed lines. The cutoff value for the formation of a hydrogen bond is 3.5 Å.

Figure 4. Ligand–residue interaction energies from MM-GBSA energy decomposition for compound **3**-hAChE (A) and compound **3**-hBChE (B). Delta Gsubtotal represents total estimated binding free energy for each residue. Delta Gele represents non-bonded electrostatics interactions. Delta Gvdw represents non-bonded

van der Waals interactions.

Figure 5. Cell viability in SH-SY5Y cells for compound **3** and rivastigmine. Data correspond to the mean ± SEM of different experiments performed in triplicate. *$p <$ 0.05, **$p < 0.01$, and ***$p < 0.001$ versus control.

Figure 6. Compound **3** inhibits ROS in SH-SY5Y cell lines. The results are represented in the percentage of control cells. The untreated cells were used as negative control, and curcumin was used as a positive control.

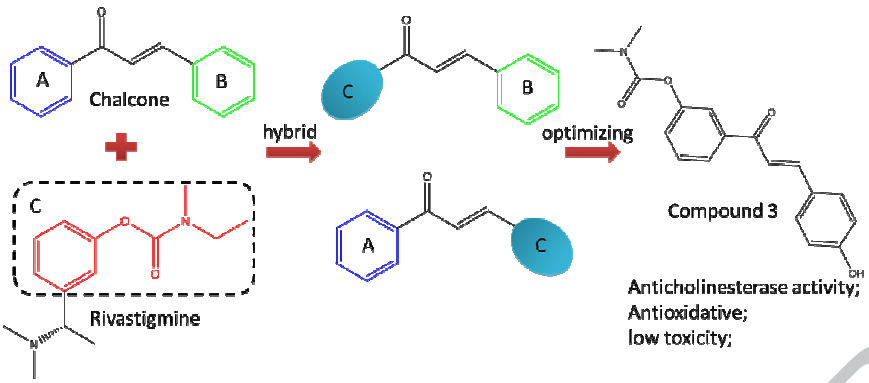

1

2

Highlights

- A series of novel chalcone-rivastigmine hybrids have been designed and synthesized.
- Biochemical assessment of cholinesterase enzyme has been carried out.
- Some of the designed compounds showed promising anticholinesterase activity and low toxicity.
- Compound **3** blocked the formation of reactive oxygen species (ROS) in SH-SY5Y cells.
- Molecular docking and molecular dynamics simulations studies have been done.